Exp Fluids (2013) 54:1537
DOI 10.1007/s00348-013-1537-z

RESEARCH ARTICLE

The influence of the arrangements of multi-sensor probe arrays on the accuracy of simultaneously measured velocity and velocity gradient-based statistics in turbulent shear flows

P. V. Vukoslavčević · J. M. Wallace

Received: 1 December 2012 / Revised: 14 March 2013 / Accepted: 7 May 2013 / Published online: 22 May 2013
© Springer-Verlag Berlin Heidelberg 2013

Abstract A highly resolved turbulent channel flow direct numerical simulation (DNS) with $Re_\tau = 200$ has been used to investigate the influence of the arrangements of the arrays (array configurations), within the sensing area of a multi-array hot-wire probe on the measurement accuracy of velocity and velocity gradient-based statistics. To eliminate all effects related to the sensor response and array characteristics (such as sensor dimensions, overheat ratio, thermal cross talk, number and orientations of the sensors and uniqueness range) so that this study could be focused solely on the effects of the array configurations (positions and separations), a concept of a perfect array was introduced, that is, one that can exactly and simultaneously measure all three velocity components at its center. The velocity component values, measured by these perfect arrays, are simply the DNS values computed at these points. Using these velocity components, the velocity and velocity gradient-based statistics were calculated assuming a linear velocity variation over the probes' sensing areas. The calculated values are compared to the DNS values for various array arrangements to study the influence of these arrangements on the measurement accuracy. Typical array configurations that previously have been used for physical probes were tested. It is demonstrated that the array arrangements strongly influence the accuracy of some of the velocity and velocity gradient-based statistics and that no single configuration exists, for a given spatial resolution, which gives the best accuracy for all of the statistics characterizing a turbulent shear flow.

P. V. Vukoslavčević
Department of Mechanical Engineering, University of Montenegro, 81000 Podgorica, Montenegro

J. M. Wallace (✉)
Burgers Program for Fluid Dynamics and Department of Mechanical Engineering, University of Maryland, College Park, MD 20742, USA
e-mail: wallace@umd.edu

1 Introduction

The first successful measurements of the velocity gradient tensor terms in turbulent flows were made by multi-sensor hot-wire probes. The operational principle of these probes is based on simultaneous measurements of velocity components at two or more points, closely separated in the flow coordinate directions. A minimum of nine hot-wire sensors are necessary to simultaneously measure all six cross-stream gradients and the three velocity components at a reference point of such multi-sensor probes. To estimate the three streamwise velocity gradients, it is necessary to apply Taylor's (1938) hypothesis of frozen turbulence or use an additional array displaced in the upstream direction. The geometry of a multi-sensor probe is defined by the arrangement of the sensors within an array (sensor configuration) and by the arrangement of the arrays within the probe sensing area (array configuration). Vukoslavčević and Wallace (2011) and Vukoslavčević (2012) have recently examined various sensor configurations. While the geometrical configurations of the sensors and their number within an array have been discussed by many authors, there hardly have been any analyses that attempt to determine the best array positions with respect to a coordinate system attached to a multi-array hot-wire probe. Typical array configurations, used to date for physically realized probes, are shown in Fig. 1.

A set of convenient abbreviations to label various configurations is given in the caption of Fig. 1. They consist of the first letters of the names of authors who designed and used them and the number of arrays for each probe. The

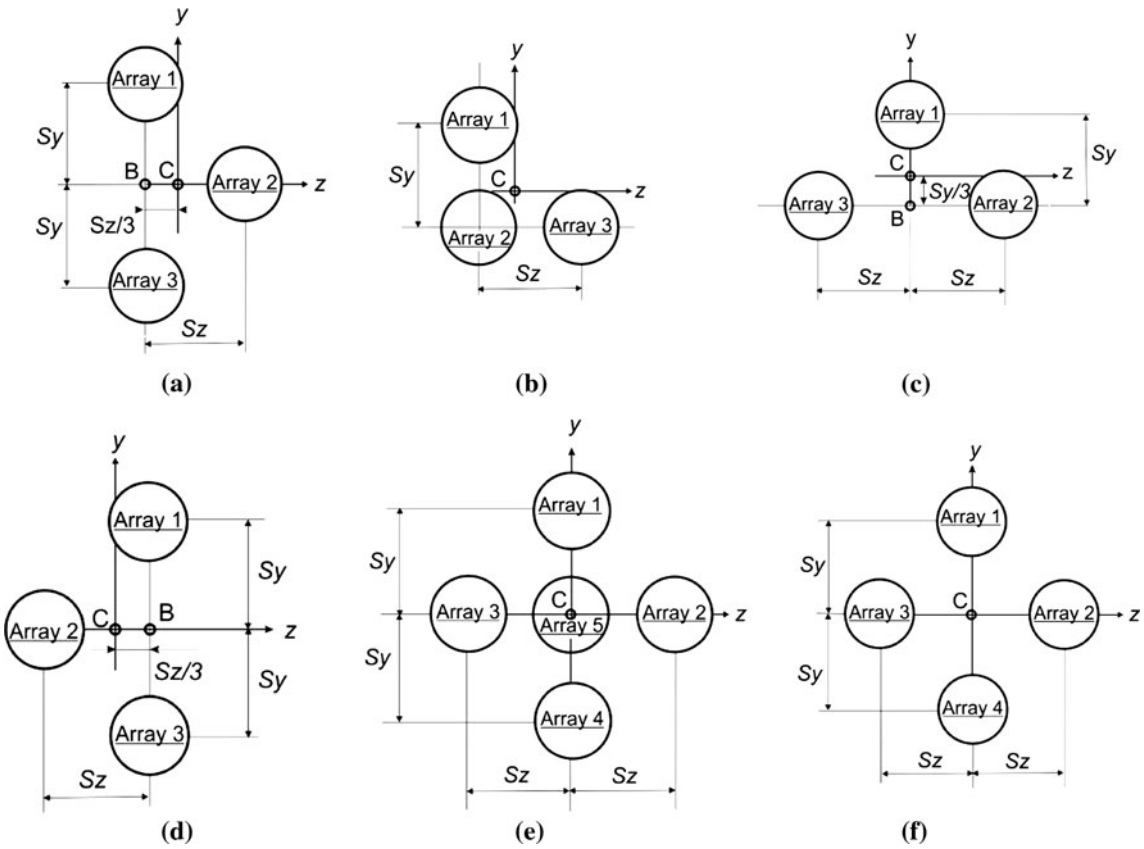

Fig. 1 Various array configurations of multi-sensor hot-wire probes: **a** VWB3, **b** TKD3, **c** VW3, **d** HA3, **e** TKD5 and **f** TKD4

configuration VWB3 was used by Vukoslavčević et al. (1991), configurations TKD3 and TKD5 by Tsinober et al. (1992), VW3 by Vukoslavčević and Wallace (1996) and HA3 by Honkan and Andreopoulos (1997). Configuration TKD4 was used by Galanti et al. (2003) and by Gulitski et al. (2007), as a part of the TKD5 configuration, but where the central array was moved upstream of the other four arrays. Symmetry appears to have been the primary motivation for the array configuration choices for the four- and five-array probes.

2 Array configuration analysis

Operation of these probes is based on the assumption that the instantaneous velocity components vary linearly over the whole probe sensing area, that is, over all the sensors. The velocity gradients are calculated using finite differences (by dividing the velocity difference between two arrays in a given direction by the distance between these arrays). In some cases, it has been assumed that the velocity varies linearly between the arrays while being constant over the sensing area of the arrays themselves. This latter assumption is only good if the array size is so small that the velocity variation over each array itself is negligible. As demonstrated by Vukoslavčević and Wallace (2011) and Vukoslavčević (2012), it is practically impossible to build a single array small enough to satisfy this assumption, which implies that the smallest length scales in various types of turbulent flows are resolved. The velocity variation between two or more arrays, placed close to each other to form a multi-array hot-wire probe, is almost never linear, especially in the near wall regions of bounded turbulent flows. Thus, the spatial arrangement of the arrays and the separation distances between them are principle characteristics of these multi-sensor hot-wire probes, affecting how well they can measure the velocity gradient tensor.

To eliminate all effects related to the sensor response and array characteristics (such as sensor dimensions, overheat ratio, thermal cross talk between sensors within an array, disturbance of the flow by the presence of the sensors and prongs, number and orientations of the sensors and uniqueness range) so that this study can be focused entirely on the effects of the array configurations (positions and separations), one can imagine perfect arrays that can exactly and simultaneously measure all three velocity components at their centers. If the velocity field varied linearly over multi-array probe sensing areas, all the array configurations presented in Fig. 1, with perfect arrays and

the same array separation distances, would give equal and accurate values of velocity and velocity gradient-based statistics. This will be the case only if the array separation is small enough to accurately assume linear velocity variation between arrays. However, as discussed above, fabricating such probes is practically impossible to achieve for even the most optimal laboratory conditions, let alone for use in field conditions. This means that the instantaneous velocity variation between arrays is almost always nonlinear even though the variations of scales above some indeterminate wavelength may be linear. If the array separations are small enough to have either concave or convex velocity variation between arrays (without second velocity derivatives being zero), this velocity variation can be illustrated by the function $f(x)$ shown in Fig. 2.

If the exact values of the function $f(x)$ at points x_1 and x_3 are known, its gradient between these points can be estimated using a finite difference expressed as $f'_{(x)} = \frac{f_{x_3} - f_{x_1}}{x_3 - x_1}$. At point x_1, the function value f_{x_1} is exact but its gradient is underestimated. At point x_3, the function is also exact but the gradient is overestimated. Finally, at point x_2, the gradient is close to the exact value, but the function $f_{x_2,c}$ that we can calculate by linear interpolation is underestimated. Thus, for a given array separation, let us say $x_3 - x_1$, at reference point x_2, we have an error of $\Delta f = f_{x_2} - f_{x_2,c}$ that we cannot avoid no matter how accurately we measure the function at points x_1 and x_3. This error will have the opposite sign if the function is concave between points x_1 and x_3. At the same reference point, the first derivative is rather accurate if the separation between x_1 and x_3 is small enough to have just a convex or concave function between these two points. A reference point does not exist with both the velocity and the velocity gradient values accurate at the same location except in the case of a linear variation of the function. From these considerations, the question arises as to where the correlation between the velocity and velocity gradient estimates will be the most accurate.

The situation becomes much more complex for the multi-array probe configurations shown in Fig. 1. Their accuracy in measuring the velocity vector and the velocity gradient tensor will depend on how the arrays are configured and the distances over which they are separated. For example, the velocity derivatives in the y-direction could be reasonably accurately estimated at point B for the array configuration shown in Fig. 1a provided that the velocity field variation in this direction is either simply concave or convex. However, the velocity gradients in the z-direction would be in error because the velocity estimate at point B would be in error.

The situation is opposite for the configuration shown in Fig. 1c. In this case, the velocity derivatives in the z-direction will be much more accurate than those in the y-direction. The configuration shown in Fig. 1d is qualitatively the same as the one in Fig. 1a; only the errors in the velocity gradients in the z-direction will have opposite signs. The configuration in Fig. 1b has both gradients in error, while the configuration in Fig. 1f estimates both gradients with the same reasonable accuracy. However, due to an additional array, this latter configuration is more difficult to fabricate compared to the three-array ones. None of these configurations has a reference point with simultaneous accuracy for both velocity and velocity gradient measurements. So it is expected that velocity–velocity gradient correlations will be in error. To avoid it, a five-array probe, shown in Fig. 1e, can be used. At the probe center, both the velocity and the velocity gradients will be the most accurate. However, the disadvantage of this configuration is its much more complex fabrication and considerably poorer spatial resolution for the same array sizes due to the additional space required for the central array.

In order to examine the characteristics of the array configurations shown in Fig. 1, a virtual experiment, using a direct numerical simulation (DNS) database, can be performed, and the best configurations to measure selective velocity and velocity gradient-based statistics can be determined.

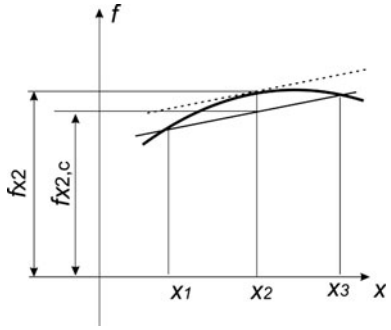

Fig. 2 A nonlinear convex function $f(x)$ between points x_1 and x_3

3 Virtual experiment

To simulate the response of hot-wire probes and to study the effects of the geometrical configurations of multi-array probes, perfect arrays can be thought of as points arranged in the appropriate probe geometry and located on the mesh of a DNS. The relative positions of these points, for a specific configuration and defined by the distances S_y and S_z from the probe center C to the array centers, are specified in Fig. 1. The velocity component values, measured by these perfect arrays, are the DNS values computed at these points.

To obtain a highly resolved DNS, a minimal turbulent channel flow, similar to that of Jiménez and Moin (1991),

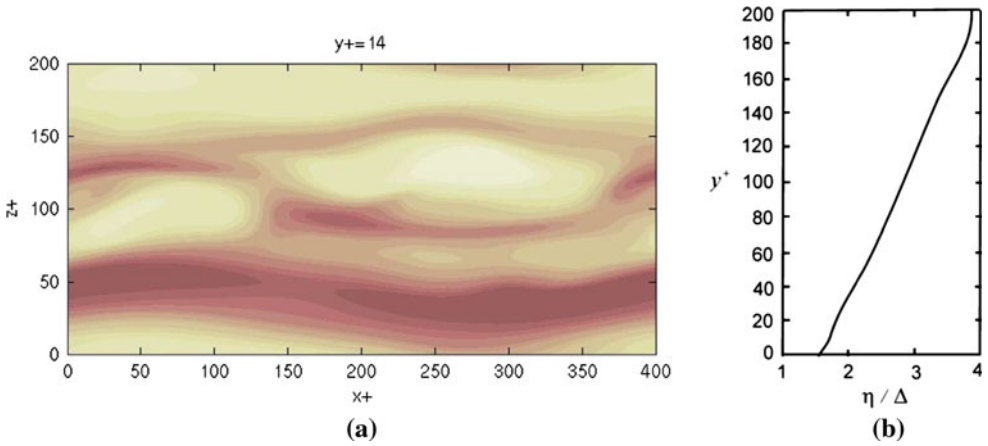

Fig. 3 **a** Contours of the streamwise velocity fluctuations in the minimal turbulent channel flow showing low- and high-speed streaks. **b** Comparison of the grid size, Δ, to the Kolmogorov length, η, across the channel

was simulated for a Reynolds number $Re_\tau = 200$ where, $Re_\tau = u_\tau h/\nu$, u_τ is the friction velocity and h is the channel half-width. The equations of motion were solved using a fractional step method, where both the advective and diffusive terms were treated explicitly using an Adams–Bashforth scheme. All spatial derivatives were discretized with second-order, central finite differences on a staggered grid. The details of the numerical methodology can be found in Piomelli et al. (2000), and the first use of this database for this type of study was by Vukoslavčević et al. (2009). The size of the computational domain was set to 2h × 2h × h and was discretized using 400 × 400 × 200 grid nodes in the streamwise, wall normal and spanwise directions, respectively. The grid was uniform in all directions, and the resulting resolution is $\Delta x^+ = \Delta y^+ = \Delta z^+ \approx 1$, where "+" denotes normalization with the viscous length ν/u_τ. This permits the existence of about two low- and high-speed streaks in the minimal channel, as can be seen in Fig. 3a. The variation of the Kolmogorov length, η, across the channel for this fixed grid spacing is shown in Fig. 3b. Near the wall, the grid size is a little less than two-thirds of the Kolmogorov length in each coordinate direction and a little more than one-quarter of this length at the channel centerline.

To be able to perform the virtual probe experiments, a database of ∼50 statistically independent instantaneous realizations over 15 eddy turnover times was generated. This sample size was found to be sufficient to obtain reasonably, but not completely, converged statistics.

A virtual probe with the "TKD4" configuration and array distances $S_y^+ = S_z^+ = 4$ from the probe center C is shown in Fig. 4.

When the array centers coincide with the nodes of the grid, the velocity components at each array center are equal to the velocity components from the DNS. Otherwise, the velocity components at the array centers can be found by an adequate interpolation. The same approach has been used for the other array configurations shown in Fig. 1

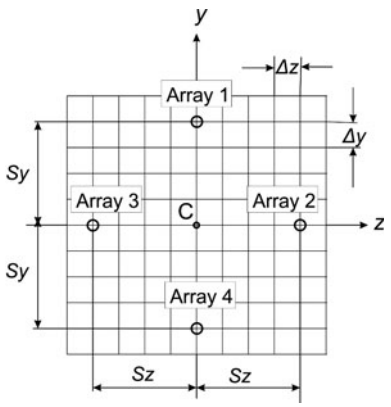

Fig. 4 Sketch of a "TKD4" configuration with arrays shown as points on the DNS grid with $\Delta x^+ = \Delta y^+ = \Delta z^+ \approx 1$ resolution

where the same spatial resolution (the distances between arrays) was maintained, that is $S_y^+ = S_z^+ = 4$ and $\Delta^+ = 1$. It follows from Fig. 3b that for this channel flow DNS, $\eta/\Delta \approx 1.6$ at $y^+ = 15$, so that $S_y/\eta = S_z/\eta = 2.5$. This means that the separations of the array centers from each other are about 5η. These values increase closer to the wall and decrease toward the channel centerline. This resolution is sufficient to place any of the sensor configurations within an array with the distance from the array center to the sensor centers of $b^+ = 2$, which is close to or better than the best spatial resolution of any of the probes used in the experiments cited in Sect. 1. The separations discussed above are used in the analysis below. Due to the dimension of the central array of the "TKD5" configuration, given in Fig. 1, the distance from the probe to the arrays' centers should be slightly increased in this case, depending on the sensor configuration within an array, and an average value of $S_y^+ = 5.2\,\Delta^+$ should be sufficient for most of the sensor configurations used so far.

By comparing the statistical properties of the simulated flow "measured" in this way by the various array configurations of virtual probes to the same properties determined

directly from the DNS, the influence of the geometrical arrangements of the probe arrays, for a given spatial resolution, can be systematically examined. In addition, by varying the separations of the arrays, for a given arrangement of the probe's arrays, the effects of spatial resolution can also be analyzed. Because the configuration TKD3, shown in Fig. 1b, does not yield the best $\partial/\partial y$ or $\partial/\partial z$ gradient values, this configuration is not presented here.

4 Velocity component statistics

The effect on the mean streamwise velocity of varying the array configurations is quite small and thus is not shown here. In Fig. 5, the rms distribution of the three velocity components at the probes' centers, denoted by the Cs in Fig. 1, is compared to the DNS values. These rms values are labeled u', v' and w', and, as explained above, they have been calculated assuming each array responds perfectly to the DNS flow field, that is, that each array "measures" the DNS value exactly. The differences from the DNS distributions are thus only due to the nonlinearity of the flow field over the probe sensing area which is not accounted for by the finite difference approximations of the velocity gradients.

It is easy to demonstrate that the configurations VWB3 and HA3 give the same results, so results from the latter are not shown. The configuration TKD5, with arrays that measure the velocity components correctly at the probe center, will give the same results as the DNS, so they are not shown either. It is evident that the rms values for all the other configurations shown in Fig. 1 are close to each other. The VW3 configuration gives slightly better results due to its better spatial resolution in the y-direction compared to the VWB3 and TKD4 configurations. To illustrate the effect of spatial resolution, the results obtained by a 50 % larger VW3 probe configuration with $S_y^+ = S_z^+ = 6$ are also shown. This configuration is much easier to fabricate, and other factors that affect the real probe response, like thermal cross talk between the sensors, and thickness and separation of the prongs, will be smaller with this arrangement. Unfortunately, the rms attenuation is significantly greater than for the smaller array separation. Similar effects are observed if the other configurations are similarly enlarged.

Skewness and flatness factors for the velocity fluctuations are shown in Figs. 6 and 7. As for the rms values, the VW3 configuration gives the best results. A relatively strong effect of the probe spatial resolution on some of these properties, particularly on F_v, for the VW3 configuration with the larger array separations can also be observed in the near the wall region.

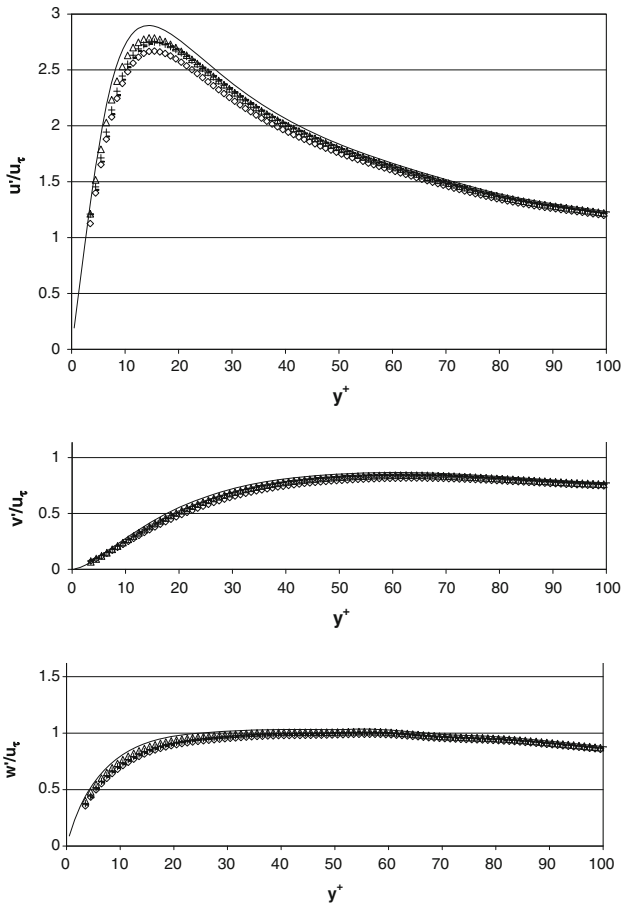

Fig. 5 Effects of the array configurations, shown in Fig. 1, on the velocity component rms values: *Solid line* DNS, *triangle* VW3, *dash* VWB3, *plus* TKD4, all with $S_y^+ = S_z^+ = 4$, *diamond* VW3, with $S_y^+ = S_z^+ = 6$

5 Vorticity component statistics

The effects of the array configurations on the vorticity component rms values are shown in Fig. 8.

The rms of ω_x is most accurately estimated with the VW3 configuration because this arrangement has the best resolution in the y-direction. The accuracy of this vorticity component with the VWB3, TKD4 and HA3 configurations is practically the same because they all have similar resolution in the y-direction. The VWB3 and HA3 configurations overestimate the rms of ω_y quite considerably near the wall. This is due to the relative poor estimate of the U velocity component at point B with these configurations. It is clear from Fig. 2 that, due to the large variation of the mean velocity gradient with distance from the wall, the value of U at point B is underestimated, resulting in a positive error of the $\partial U/\partial z$ gradient for the VWB3 configuration and a negative one for the HA3 configuration. The error of the rms values of ω_y will be positive in both cases. For these configurations, these inaccuracies also

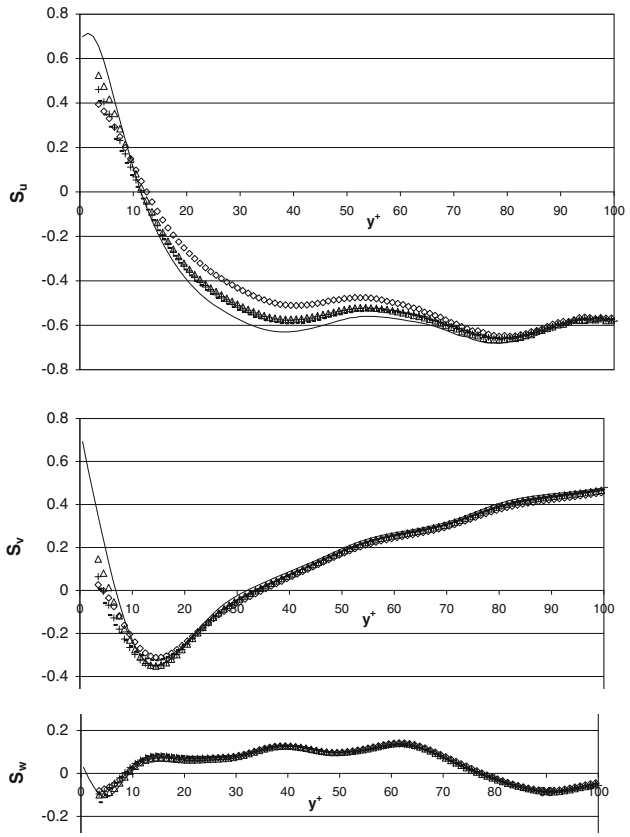

Fig. 6 Effects of the array configurations on the velocity component skewness factors: *Solid line* DNS, *triangle* VW3, *dash* VWB3, *plus* TKD4, all with $S_y^+ = S_z^+ = 4$, *diamond* VW3 with $S_y^+ = S_z^+ = 6$

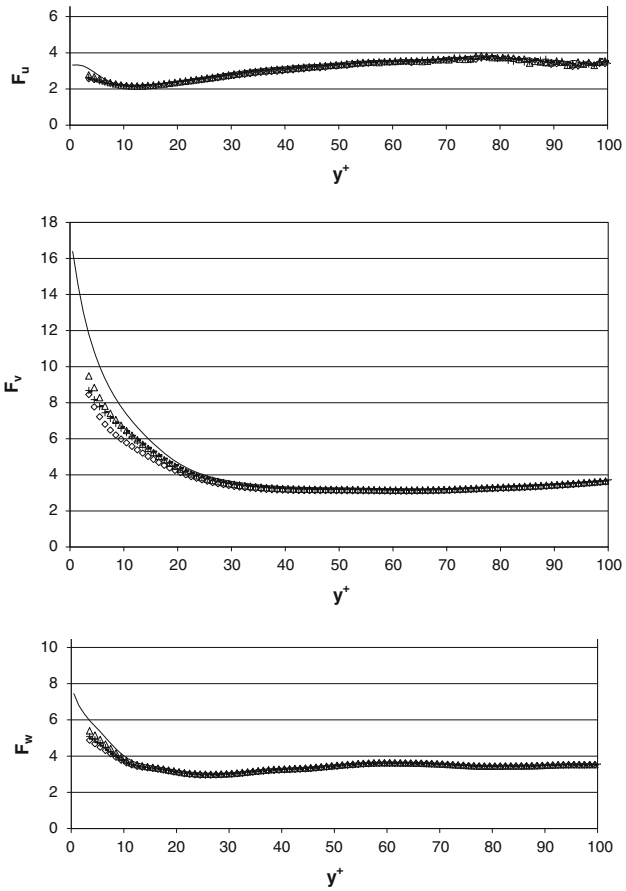

Fig. 7 Effects of the array configurations on the velocity component flatness factors: *Solid line* DNS, *triangle* VW3, *dash* VWB3, *plus* TKD4, all with $S_y^+ = S_z^+ = 4$, *diamond* VW3 with $S_y^+ = S_z^+ = 6$

strongly affect the values of the skewness of ω_y, as shown in Fig. 9. As expected, near the wall, the skewness of ω_y for VWB3 has a large positive error, and for HA3, the error is large and negative.

The strong influence of spatial resolution can be observed from the rms values of ω_x for the TKD5 configuration. The central array of this configuration does not play a role in the vorticity measurement, so, for the purposes of this analysis, this configuration is the same as the TKD4 configuration only larger in size, that is, $S_y^+ = S_z^+ = 5.2$ in comparison with $S_y^+ = S_z^+ = 4$, in order to provide space for the fifth array. This poorer spatial resolution affects both the $\partial/\partial y$ and the $\partial/\partial z$ gradients. As a consequence, the vorticity component rms values are less accurate compared to the TKD4 configuration.

The skewness of ω_y has large errors for the VWB3 and HA3 configurations for the reason discussed above, where the rms values were discussed. The errors of the skewness of ω_x have opposite signs for the same reason. The skewness of ω_z is the most accurate for the VW3 configuration because it has the best spatial resolution in the y-direction. Overall, it is clear that the vorticity statistics of the VW3 configuration are the most accurate. Adding a fourth array, as was done for the TKD4 configurations, improves ω_y' only in the region very close to the wall but has deleterious effects for most of the other statistics.

The skewness and flatness distributions of the vorticity components, shown in Figs. 9 and 10, as well as the skewness distributions of the velocity components, do not vary as smoothly as expected. This is probably due to a somewhat too small data sample size for these higher order statistics to obtain complete statistical convergence.

6 Velocity–vorticity correlation statistics

The $\overline{w\omega}_y - \overline{v\omega}_z$ velocity–vorticity correlation is equal to the y-gradient of the Reynolds shear stress for plane turbulent channel flow, as discussed by Klewicki (1989) and Klewicki et al. (1994). This correlation, obtained for the various array configurations, is compared to the DNS values in Fig. 11.

The best agreement is obtained for the TKD4 configuration. Although the TKD5 configuration measures the

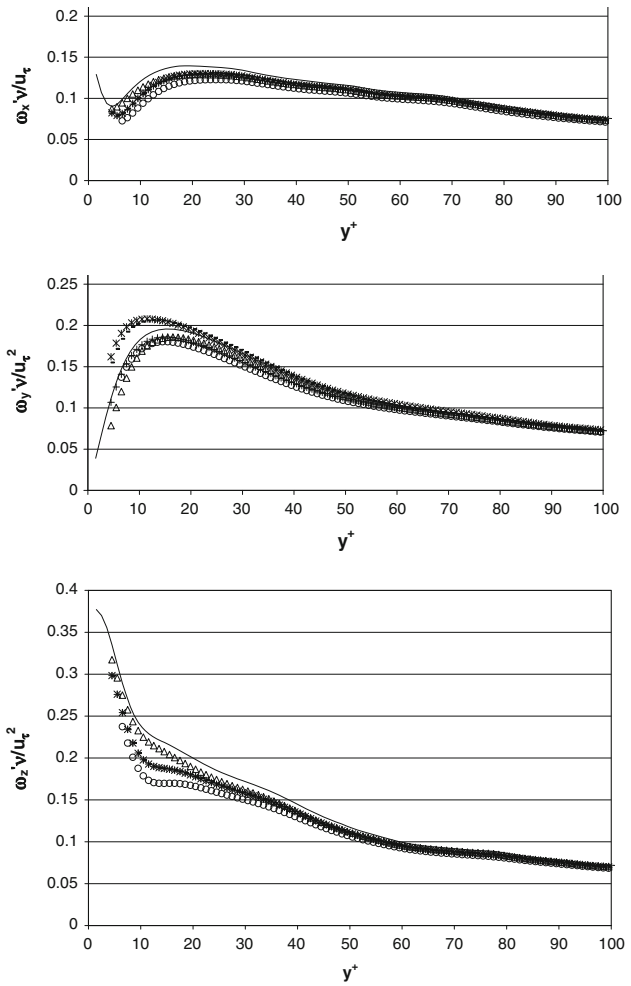

Fig. 8 Effects of the array configurations on the vorticity component rms values: *Solid line* DNS, *triangle* VW3, *dash* VWB3, *plus* TKD4, *star* HA3, all with $S_y^+ = S_z^+ = 4$; *circle* TKD5 with $S_y^+ = S_z^+ = 5.2$

velocity much more accurately than the TKD4 configuration because of the fifth array placed at the probe center, the velocity–vorticity correlation is not as good due to the larger array separations. The VWB3, VW3, HA3 configurations do not perform very well. The worse is the VW3 configuration. For this configuration, the calculated value of ω_y will be close to the induced value at point B. This is because the calculated value of the $\partial u/\partial z$ gradient is most accurate at that point. Similarly, the calculated value of ω_z will be the most accurate at a point half the distance between point B and array 1. However, these vorticity component values are not accurate at point C where we calculate their correlation with the velocity component values. As a consequence, the correlation is in error. A similar situation occurs for the VWB3 and HA3 configurations, but the error is smaller because the variation of the instantaneous values of the vorticity components between points B and C is smaller for these configurations.

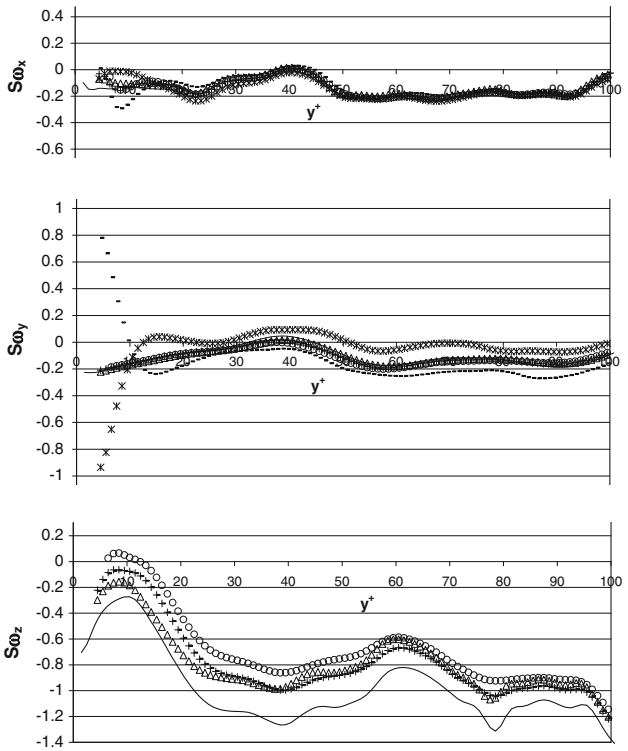

Fig. 9 Effects of the array configurations on the vorticity component skewness factors: *Solid line* DNS, *triangle* VW3, *dash* VWB3, *plus* TKD4, *star* HA3, all with $S_y^+ = S_z^+ = 4$; *circle* TKD5 with $S_y^+ = S_z^+ = 5.2$

7 Turbulent kinetic energy dissipation and production rates

As Fig. 12 shows, the TKD4 and TKD5 configurations measure the production rate much more accurately than the dissipation rate. Keeping in mind that the production rate for the fully developed channel flow is given by $P = -\overline{uv}\partial\bar{U}/\partial y$, this means that they measure the Reynolds shear stress distribution accurately, as can be seen in Fig. 13.

The opposite result is the case for the VW3 configuration. This configuration does not accurately measure the Reynolds shear stress, as was the case for the velocity–vorticity correlations shown in Fig. 12, but the accuracy of the dissipation rate measurement for this configuration is reasonable. The best results for both the dissipation and the production rates are obtained with the VWB3 and HA3 configurations. The dissipation rate is calculated from the full tensorial expression.

8 Streamwise velocity gradients

All of the multi-array hot-wire probe configurations shown in Fig. 1 can simultaneously measure the six cross-stream velocity gradients. The only array configuration shown in

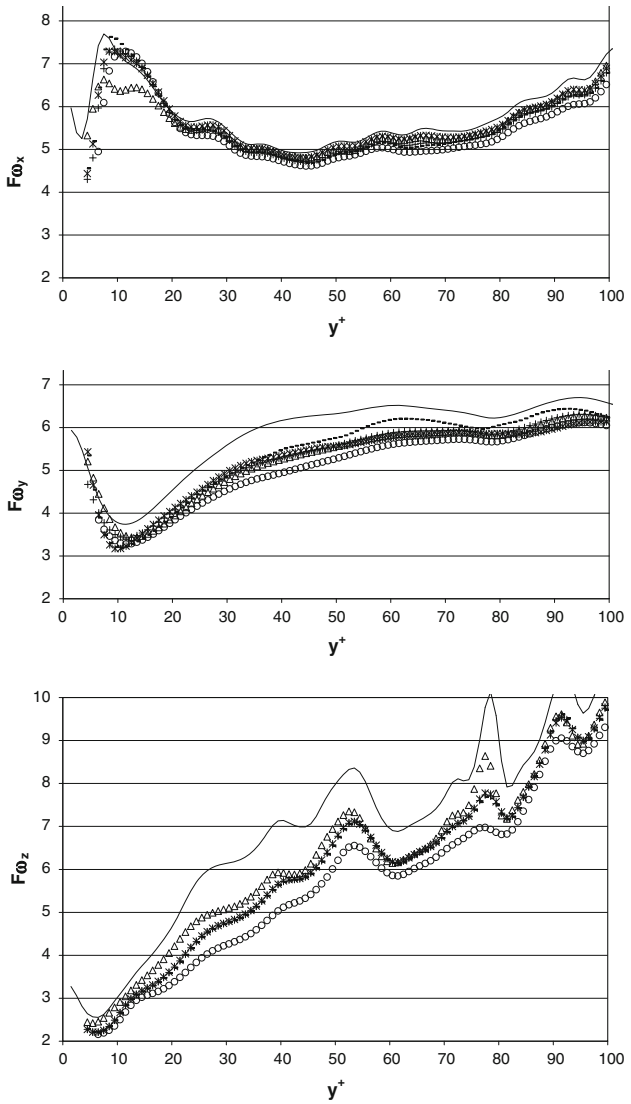

Fig. 10 Effects of the array configurations on the vorticity component flatness factors: *Solid line* DNS, *triangle* VW3, *dash* VWB3, *plus* TKD4, *star* HA3, all with $S_y^+ = S_z^+ = 4$; *circle* TKD5 with $S_y^+ = S_z^+ = 5.2$

the figure that can also be used to directly measure the three streamwise gradients simultaneously is the TKD5 configuration with the central array placed forward (upstream) of the other four arrays at some distance S_x. For all the other configurations, the simultaneous estimates of the three streamwise velocity gradients, $\partial U_i/\partial x$, must rely on Taylor's (1938) hypothesis of frozen turbulence or a refined form of this hypothesis obtained from the momentum equation by neglecting the pressure and viscous terms, as discussed by Wallace and Vukoslavčević (2009) (for a fuller discussion of Taylor's hypothesis, see Tropea et al. 2007, pp. 422–425).

Using the TKD5 configuration, with the central array placed forward (upstream) at a distance S_x, the velocity

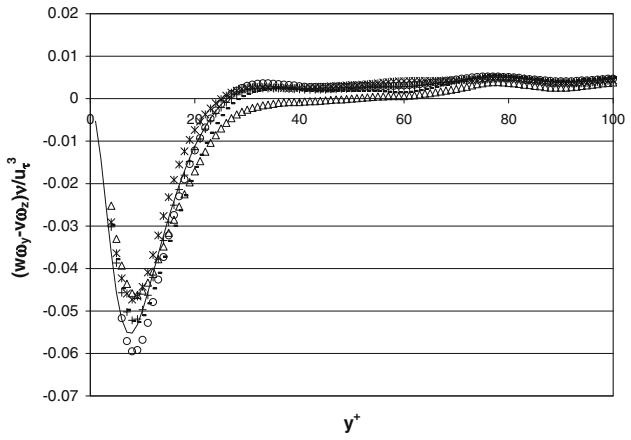

Fig. 11 Effects of the array configurations on the $\overline{w\omega}_y - \overline{v\omega}_z$ values: *Solid line* DNS, *triangle* VW3, *dash* VWB3, *plus* TKD4, *star* HA3, all with $S_y^+ = S_z^+ = 4$; *circle* TKD5 with $S_y^+ = S_z^+ = 5.2$

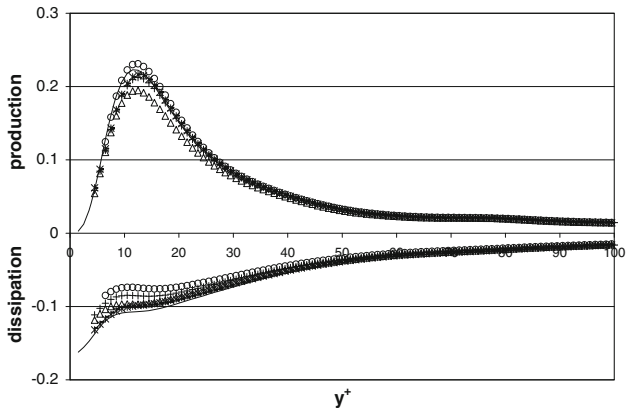

Fig. 12 Effects of the array configurations on the production and dissipation rates: *Solid line* DNS, *triangle* VW3, *dash* VWB3, *plus* TKD4, *star* HA3, all with $S_y^+ = S_z^+ = 4$; *circle* TKD5 with $S_y^+ = S_z^+ = 5.2$

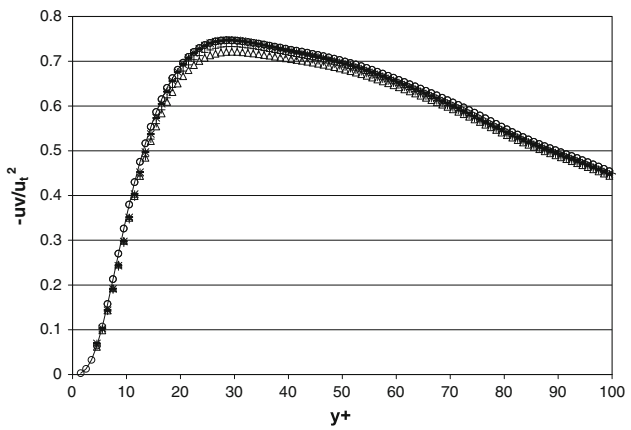

Fig. 13 Effects of the array configurations on the Reynolds shear stress distribution: *Solid line* DNS, *triangle* VW3, *dash* VWB3, *plus* TKD4, *star* HA3, all with $S_y^+ = S_z^+ = 4$; *circle* TKD5 with $S_y^+ = S_z^+ = 5.2$

components can be determined at two points that are close to each other and separated along the x-axis, that is, measured at the center of the central array and estimated by interpolation at point C in Fig. 1e in the plane through the centers of the other four arrays and from their measured values. This approach was used by Galanti et al. (2003) and Gulitski et al. (2007). The measurement accuracy of this approach depends on the accuracy of the velocity measurements at the center of each of the five arrays and the array separations S_x, S_y and S_z from point C in Fig. 1e. As before, assuming a perfect array response, the influence of the array separations on the measurement accuracy can be isolated and tested.

To do this, the array separation in the x-direction was chosen as $S_x^+ = 4$, that is, the same as the distances S_y and S_z of configuration TKD4 in Fig. 1. This is the minimum separation in the x-direction for the distance from the array to the sensor centers of $b^+ = 2$. However, in order to avoid wake interference from the upstream array on the other four arrays, they must be moved further from the center C in the y- and z-directions. This means that the minimal array separation of the TKD5 configuration with the *central array* moved upstream and $b^+ = 2$ for this analysis is $S_x^+ = 4$, $S_y^+ = S_z^+ = 8$. The comparison of the DNS with the "measured" (by such a virtual probe) streamwise velocity gradients is shown in Fig. 14.

The rms distributions of all three velocity gradients are overestimated and badly in error. The $\partial u/\partial x$ component is especially badly overestimated. This is not surprising because the rms of the velocity component at the probe center of the TKD4 configuration is underestimated, as can be seen in Fig. 5, where they are shown for the $S_z^+ = S_z^+ = 4$ array separations. With array separations of $S_z^+ = S_z^+ = 8$, as in this case, the rms values of the velocity components at location C will be much more underestimated, and, as a consequence, the rms of the streamwise velocity component gradients will be badly overestimated. It is clear that the measurement of the streamwise velocity gradients by such a configuration is not reliable. Moreover, it is hard to imagine any multi-sensor hot-wire probe configuration that can simultaneously measure all three velocity gradients in the x-direction with sufficient accuracy while also accurately measuring the cross-stream gradients. Thus, it seems necessary to rely on Taylor's (1938) frozen turbulence hypothesis.

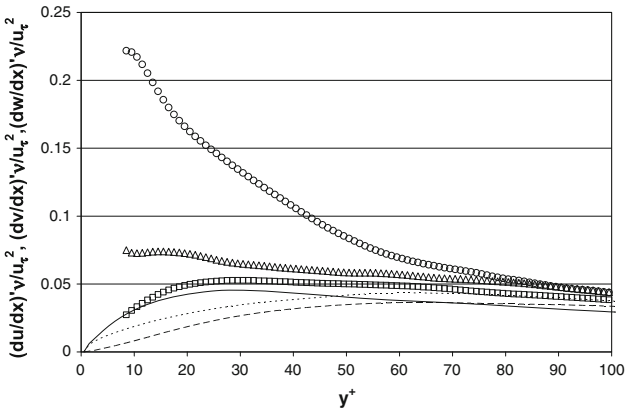

Fig. 14 Comparison of the DNS and "measured" rms distributions of the streamwise velocity gradients of the TKD5 array configuration with the central array moved upstream. DNS: *Solid line*, $\partial u/\partial x$; *dashed line*, $\partial v/\partial x$; *dotted line*, $\partial w/\partial x$. TKD5: *circle*, $\partial u/\partial x$; *square*, $\partial v/\partial x$; *triangle*, $\partial w/\partial x$, with $S_x^+ = 4$ and $S_y^+ = S_z^+ = 8$

A method to test this hypothesis for each of the array configurations shown in Fig. 1 is to determine the streamwise gradient of U from the continuity equation for incompressible flow,

$$\left(\frac{\partial U}{\partial x}\right)_c = -\frac{\partial V}{\partial y} - \frac{\partial W}{\partial z}, \tag{1}$$

and compare this value to the value obtained from Taylor's hypothesis,

$$\left(\frac{\partial U}{\partial x}\right)_T = -\frac{1}{U_{\text{con}}}\frac{\partial U}{\partial t}, \tag{2}$$

where U_{con} is a convection velocity, usually taken as a fraction of the local mean velocity, $\overline{U}$, or as the local instantaneous velocity, U. In order to use this possibility and determine appropriate values of the convective velocity U_{con}, the rms of $\left(\frac{\partial U}{\partial x}\right)_c$, obtained from the continuity Eq. (1), should be determined with sufficient accuracy. The rms determined from continuity and the DNS values of this gradient are compared in Fig. 15, for the configurations shown in Fig. 1.

Very good agreement is obtained for the VW3 configuration. The configurations VWB3 and HA3 are considerably in error for the reason explained in Sect. 5. The configurations TKD4 and TKD5 are worse than VW3, which is obviously due to their poorer spatial resolution. The differences between the TKD4 and TKD5 configurations are due to spatial resolution only, because the central array of TKD5 configuration does not play any role in the spanwise gradient determination.

To make sure that the streamwise velocity gradient obtained from the continuity equation is close to the DNS values, not only should their rms values agree well with each other (an amplitude measure) but also the phase shift between their signals should be close to zero. In order to check that, the correlation coefficient

$$K_{\left(\frac{\partial U}{\partial x}\right)_c\left(\frac{\partial U}{\partial x}\right)} = \frac{\overline{\left(\frac{\partial U}{\partial x}\right)_c\left(\frac{\partial U}{\partial x}\right)}}{\left(\frac{\partial U}{\partial x}\right)_c'\left(\frac{\partial U}{\partial x}\right)'} \tag{3}$$

was determined and is shown in Fig. 16 for the various configurations.

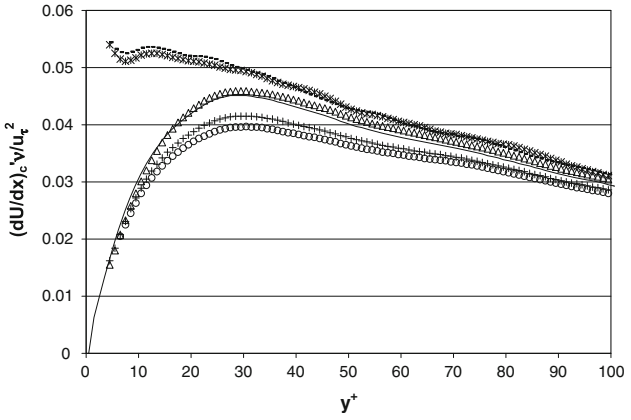

Fig. 15 Effects of the array configurations on the rms values of the streamwise velocity gradient $(\partial U/\partial x)_c$, obtained from continuity: *Solid line* DNS, *triangle* VW3, *dash* VWB3, *plus* TKD4, *star* HA3, all with $S_y^+ = S_z^+ = 4$; *circle* TKD5 with $S_y^+ = S_z^+ = 5.2$

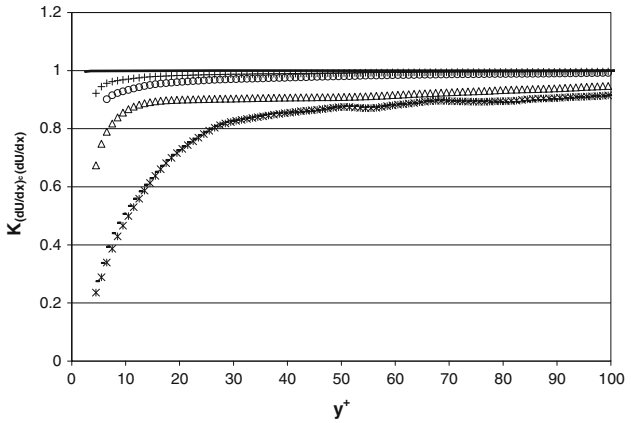

Fig. 16 Effects of the array configurations on the phase shift of the "measured" streamwise velocity gradient $(\partial U/\partial x)_c$: *Solid line* DNS, *triangle* VW3, *dash* VWB3, *plus* TKD4, *star* HA3, all with $S_y^+ = S_z^+ = 4$; *circle* TKD5 with $S_y^+ = S_z^+ = 5.2$

The signals obtained with TKD4 and TKD5 configurations are in reasonably good phase agreement with the DNS values, even close to the wall, probably due to the symmetry of their configurations with respect to the coordinate axes. The signal obtained with the VW3 configuration is in adequate phase agreement for $y^+ > 10$. The signals obtained by the VWB3 and HA3 configurations are completely out of phase in the near wall region.

It can be concluded that the VW3 configuration could be used to determine the streamwise velocity gradients, $\partial U/\partial x$, with reasonable amplitude and phase agreement for $y^+ > 10$. The phase agreement of the signals obtained with the TKD4 and TKD5 configurations is excellent, but the rms of these signals are attenuated by about 10 % around $y^+ = 30$. It appears that all three of these configurations can be used to determine the streamwise velocity gradients by applying Taylor's hypothesis with much better accuracy than by obtaining it with direct measurements using a five-array probe.

9 Conclusions

1. The array configurations of multi-array hot-wire probes strongly influence the accuracy of most velocity and velocity gradient-based statistics.
2. For a given spatial resolution, no unique configuration exists that gives the best accuracy for all of the statistics characterizing turbulent shear flow.
3. Some of the arrangements, notably the one denoted as VW3, measure the velocity and velocity gradient statistics with reasonable accuracy, but velocity–velocity gradient correlations can be significantly in error with this array configuration.
4. The geometrical symmetry of the array arrangements strongly influences the measurement accuracy of the velocity component correlations and the velocity–velocity gradient correlations.
5. It appears to be extremely difficult to *directly* measure, with reasonable accuracy, the streamwise velocity gradients simultaneously with the cross-stream gradients using multi-array hot-wire probes.
6. In order to determine the streamwise velocity gradients, it is possible to employ Taylor's hypothesis with reasonable accuracy.

Acknowledgments This research was supported by the Ministry of Science and Education of Montenegro. The authors also wish to thank Nicolas Beratlis and Elias Balaras who provided the DNS database used in this investigation.

References

Galanti B, Gulitski G, Kholmyansky M, Tsinober A, Yorish S (2003) Velocity derivatives in turbulent flows in an atmospheric boundary layer without Taylor hypothesis. Turbul Shear Flow Phenom 2:745–750

Gulitski G, Kholmyansky M, Kinzelbach W, Luthi B, Tsinober A, Yorish S (2007) Velocity and temperature derivatives in high-Reynolds number turbulent flows in the atmospheric surface layer. Part 1. Facilities, methods and some general results. J Fluid Mech 589:57–81

Honkan A, Andreopoulos Y (1997) Vorticity, strain rate and dissipation characteristics in the near wall region of turbulent boundary layers. J Fluid Mech 350:29–96

Jiménez J, Moin P (1991) The minimal flow unit in near-wall turbulence. J Fluid Mech 225:213–240

Klewicki J (1989) Velocity–vorticity correlations related to the gradients of the Reynolds stress in parallel turbulent wall flows. Phys Fluids A 1:1285–1288

Klewicki J, Murray J, Falco R (1994) Vortical motion contributions to stress transport in turbulent boundary layers. Phys Fluids 6:277–286

Piomelli U, Balaras E, Pascarelli A (2000) Turbulent structures in accelerating boundary layers. J Turbul 1:N1. doi:10.1088/1468-5248/1/1/001

Taylor GI (1938) Production and dissipation of vorticity in a turbulent fluid. Proc R Soc Lond 164:15–23

Tropea C, Foss JF, Yarin A (2007) Springer handbook of experimental fluid mechanics. Springer, Berlin

Tsinober A, Kit E, Dracos T (1992) Experimental investigation of the field of velocity gradients in turbulent flows. J Fluid Mech 242:169–192

Vukoslavčević PV (2012) A hot wire probe configuration and data reduction method to minimize velocity gradient errors for simultaneous measurement of three velocity components in turbulent flows. Exp Fluids 53:481–488

Vukoslavčević P, Wallace JM (1996) A 12-sensor hot-wire probe to measure the velocity and vorticity vectors in turbulent flow. Meas Sci Technol 7:1451–1461

Vukoslavčević PV, Wallace JM (2011) On the accuracy of simultaneously measuring velocity component statistics in turbulent wall flows with arrays of three or four hot-wire sensors. Exp Fluids 51:1509–1516

Vukoslavčević P, Wallace JM, Balint JL (1991) The velocity and vorticity vector fields of a turbulent boundary layer. Part 1. Simultaneous measurement by hot wire anemometry. J Fluid Mech 228:25–52

Vukoslavčević PV, Beratlis N, Balaras E, Wallace JM, Sun O (2009) On the spatial resolution of velocity and velocity gradient-based turbulence statistics measured with multi-sensor hot-wire probes. Exp Fluids 46:109–119

Wallace JM, Vukoslavčević PV (2009) Measurement of the velocity gradient tensor in Turbulent Flows. Ann Rev Fluid Mech 42:157–181